Journal of Computational Physics 245 (2013) 43–61

Contents lists available at SciVerse ScienceDirect

Journal of Computational Physics

journal homepage: www.elsevier.com/locate/jcp

An inverse Lax–Wendroff method for boundary conditions applied to Boltzmann type models ☆

Francis Filbet *, Chang Yang

Université de Lyon, Institut Camille Jordan, CNRS-UMR 5208, Université Claude Bernard, Lyon 1, 43 Boulevard 11 Novembre 1918, F-69622 Villeurbanne cedex, France

ARTICLE INFO

Article history:
Received 13 September 2012
Received in revised form 4 February 2013
Accepted 7 March 2013
Available online 26 March 2013

Keywords:
Inverse Lax–Wendroff procedure
WENO
Boltzmann type models

ABSTRACT

In this paper we present a new algorithm based on Cartesian meshes for the numerical approximation of kinetic models set in an arbitrary geometry. Due to the high dimensional property of kinetic models, numerical algorithms based on unstructured meshes are not really appropriate since most of numerical methods (semi-Lagrangian, spectral methods) are particularly efficient on structured grids. Here we propose to adapt the inverse Lax–Wendroff procedure, which has been recently introduced for conservation laws [21], for kinetic equations. Numerical simulations in $1D \times 3D$ and $2D \times 3D$ based on this approach are proposed for Boltzmann type operators (BGK, ES-BGK models).

© 2013 Elsevier Inc. All rights reserved.

1. Introduction

We are interested in the numerical approximation of solutions to kinetic equations set in an arbitrary geometry with different type of boundary conditions. Unfortunately, classical structured or unstructured meshes are not appropriate due to the high dimensional property of kinetic problems. In contrast, the Cartesian grids make numerical methods efficient and easy to implement. The difficulty is that obviously grid points are usually not located on the physical boundary when using a Cartesian mesh, thus a suitable numerical method to capture the boundary condition is required. Several numerical methods based on Cartesian meshes have been developed in computational fluid dynamics in last decade. Among these methods, the immersed boundary method (IBM), first introduced by Peskin [18] for the study of biological fluid mechanics problems, has attracted considerable attention because of its use of a regular Cartesian grid and great simplification of tedious grid generation task. The basic idea of the immersed boundary method is that the effect of the immersed boundary on the surrounding fluid is represented through the introduction of some forcing terms in the momentum equations. The extension of IBM methods has been then developed in [2,14]. For conservation laws, two major classes of immersed boundary methods can be distinguished on different discretization types. The first one is the Cartesian cut-cell method [12], which is based on a finite volume approach. This conceptually simple technique "cuts" solid bodies out of a background Cartesian mesh. Thus we get several polygons (cut-cells) around the boundary. Then the numerical flux at the boundary of these cut-cells are imposed using the real boundary conditions. This method satisfies well the conservation laws, however to determine the polygons is still a delicate issue. The second class is based on a finite difference method. To achieve a high order interior scheme, several ghost points behind the boundary are added. For instance for solving hyperbolic conservations laws, an inverse Lax–Wendroff type procedure is used to impose some artificial values at ghost points [21]. The idea of the inverse

☆ The authors are partially supported by the European Research Council ERC Starting Grant 2009, project 239983-*NuSiKiMo*.
* Corresponding author. Tel.: +33 4 72 44 62 62.
E-mail addresses: filbet@math.univ-lyon1.fr (F. Filbet), yang@math.univ-lyon1.fr (C. Yang).

0021-9991/$ - see front matter © 2013 Elsevier Inc. All rights reserved.
http://dx.doi.org/10.1016/j.jcp.2013.03.015

Lax–Wendroff procedure (ILW) is to use successively the partial differential equation to write the normal derivatives at the boundary in terms of the tangential and time derivatives of the given boundary conditions. From these normal derivatives, we can obtain accurate values of ghost points using a Taylor expansion of the solution at the point located on the boundary.

The goal of this paper is to extend the inverse Lax–Wendroff procedure to kinetic equations together with an efficient time discretization technique [6,7] for problems where boundary conditions play a significant role. In particular, we are interested in low speed and low Knudsen flows for which Direct Simulation Monte-Carlo methods (DSMC) are unsuitable due to the requirement to perform large amounts of data sampling in order to reduce the statistical noise.

For simplicity, we only consider simple collision operators as the ellipsoidal statistics BGK (ES-BGK) model introduced by Holway [10]. This model gives the correct transport coefficients for Navier-Stokes system of equations, so that Boltzmann or ES-BGK simulations are expected to give the same results for dense gases. Moreover, Filbet and Jin recently proposed a deterministic asymptotic preserving scheme for the ES-BGK model, where the entire equation can be solved explicitly and it can capture the macroscopic fluid dynamic limit even if the small scale determined by the Knudsen number is not numerically resolved [8]. We will use this scheme to solve ES-BGK model while on the boundary the inverse Lax–Wendroff procedure will be applied.

The outline of the paper is as follows. In Section 2 we describe precisely the inverse Lax–Wendroff procedure for the Maxwell's boundary conditions in 1D and 2D space dimension. Then in Section 3 we present the ES-BGK model and the application of inverse Lax–Wendroff procedure to this model. In Section 4 various numerical examples are provided in $1D \times 3D$ and $2D \times 3D$ to demonstrate the interest and the efficiency of our method in term of accuracy and complexity. Finally a conclusion and some perspectives are given in Section 5.

2. Numerical method for the Maxwell's boundary conditions

The fundamental kinetic equation for rarefied gas is the Boltzmann equation

$$\frac{\partial f}{\partial t} + \mathbf{v}\cdot\nabla_{\mathbf{x}} f = \frac{1}{\varepsilon}\mathcal{Q}(f), \tag{2.1}$$

which governs the evolution of the density $f(t,\mathbf{x},\mathbf{v})$ of monoatomic particles in the phase space $\Omega\times\mathbb{R}^3$, where $\mathbf{x}\in\Omega\subset\mathbb{R}^{d_{\mathbf{x}}}$, $\mathbf{v}\in\mathbb{R}^3$. The collision operator is either given by the full Boltzmann operator

$$\mathcal{Q}(f)(\mathbf{v}) = \int_{\mathbb{R}^3}\int_{\mathbb{S}^2} B(|\mathbf{v}-\mathbf{v}_\star|,\cos\theta)\left(f'_\star f' - f_\star f\right) d\sigma\, d\mathbf{v}_\star \tag{2.2}$$

or by a simplified model as the BGK or ES-BKG operator (see the next section). Boltzmann's type collision operators share the fundamental properties of conserving mass, momentum and energy: at the formal level

$$\int_{\mathbb{R}^3} \mathcal{Q}(f)\,\phi(\mathbf{v})\,d\mathbf{v} = 0, \quad \phi(\mathbf{v}) = 1, \mathbf{v}, |\mathbf{v}|^2.$$

Moreover, the equilibrium is the local Maxwellian distribution namely:

$$\mathcal{M}[f](t,\mathbf{x},\mathbf{v}) = \frac{\rho(t,\mathbf{x})}{(2\pi T(t,\mathbf{x}))^{3/2}}\exp\left(-\frac{|\mathbf{u}(t,\mathbf{x})-\mathbf{v}|^2}{2T(t,\mathbf{x})}\right),$$

where ρ, $\mathbf{u}$, T are the density, macroscopic velocity and the temperature of the gas, defined by

$$\begin{cases} \rho(t,\mathbf{x}) = \int_{\mathbb{R}^3} f(t,\mathbf{x},\mathbf{v})d\mathbf{v}, \\ \mathbf{u}(t,\mathbf{x}) = \frac{1}{\rho(t,\mathbf{x})}\int_{\mathbb{R}^3}\mathbf{v} f(t,\mathbf{x},\mathbf{v})d\mathbf{v}, \\ T(t,\mathbf{x}) = \frac{1}{3\,\rho(t,\mathbf{x})}\int_{\mathbb{R}^3}|\mathbf{u}(t,\mathbf{x})-\mathbf{v}|^2 f(t,\mathbf{x},\mathbf{v})d\mathbf{v}. \end{cases} \tag{2.3}$$

In order to define completely the mathematical problem (2.1), suitable boundary conditions on $\partial\Omega$ should be applied. Here we consider wall type boundary conditions introduced by Maxwell [15], where it is assumed that one fraction $(1-\alpha)$ of the emerging particles is reflected elastically at the wall, whereas the remaining fraction α is thermalized and leaves the wall in a Maxwellian distribution (see Fig. 1). The parameter α is called accommodation coefficient [4].

More precisely, at any $\mathbf{x}\in\partial\Omega$, the smooth boundary $\partial\Omega$ is assumed to have a unit inward normal $\mathbf{n}(\mathbf{x})$ and for $\mathbf{v}\cdot\mathbf{n}(\mathbf{x})\geqslant 0$, we assume that at the solid boundary a fraction $(1-\alpha)$ is perfectly reflected, while the remaining portion α of particles is absorbed by the wall and then re-emitted according to a velocity distribution which has the same temperature as the one at the solid wall. This is equivalent to impose for the ingoing velocities

$$f(t,\mathbf{x},\mathbf{v}) = (1-\alpha)\mathcal{R}[f(t,\mathbf{x},\mathbf{v})] + \alpha\mathcal{M}[f(t,\mathbf{x},\mathbf{v})], \quad \mathbf{x}\in\partial\Omega,\ \mathbf{v}\cdot\mathbf{n}(\mathbf{x})\geqslant 0, \tag{2.4}$$

with $0\leqslant\alpha\leqslant 1$ and

$$\begin{cases} \mathcal{R}[f(t,\mathbf{x},\mathbf{v})] = f(t,\mathbf{x},\mathbf{v}-2(\mathbf{v}\cdot\mathbf{n}(\mathbf{x}))\mathbf{n}(\mathbf{x})), \\ \mathcal{M}[f(t,\mathbf{x},\mathbf{v})] = \mu(t,\mathbf{x}) f_w(\mathbf{v}). \end{cases} \tag{2.5}$$

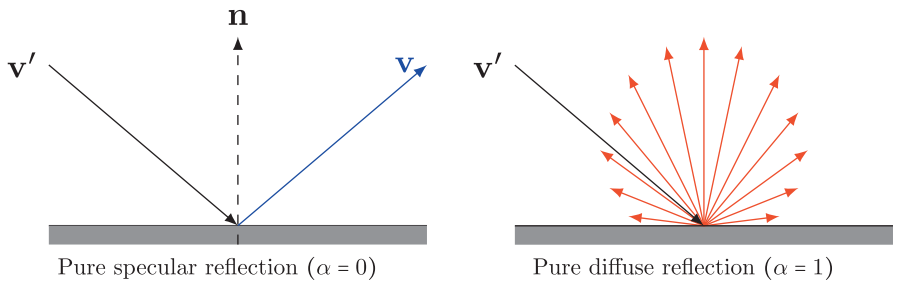

Fig. 1. Schematic representation of the Maxwell conditions at the boundary.

By denoting T_w the temperature of the solid boundary, f_w is given by

$$f_w(\mathbf{v}) := \exp\left(-\frac{\mathbf{v}^2}{2T_w}\right) \tag{2.6}$$

and the value of $\mu(t,\mathbf{x})$ is determined by mass conservation at the surface of the wall for any $t \in \mathbb{R}^+$ and $\mathbf{x} \in \partial\Omega$

$$\mu(t,\mathbf{x}) \int_{\mathbf{v}\cdot\mathbf{n}(\mathbf{x})\geqslant 0} f_w(\mathbf{v})\mathbf{v}\cdot\mathbf{n}(\mathbf{x})d\mathbf{v} = -\int_{\mathbf{v}\cdot\mathbf{n}(\mathbf{x})<0} f(\mathbf{v})\mathbf{v}\cdot\mathbf{n}(\mathbf{x})d\mathbf{v}. \tag{2.7}$$

Let us emphasize that since the velocity field is a variable, the boundary conditions have to be applied at all points $\mathbf{x} \in \partial\Omega$. The inflow corresponds to

$$\Gamma_{\text{in}} = \{(\mathbf{x},\mathbf{v}) \in \partial\Omega \times \mathbb{R}^3; \quad \mathbf{v}\cdot\mathbf{n}(\mathbf{x}) \geqslant 0\},$$

whereas the outflow corresponds to

$$\Gamma_{\text{out}} = \{(\mathbf{x},\mathbf{v}) \in \partial\Omega \times \mathbb{R}^3; \ \mathbf{v}\cdot\mathbf{n}(\mathbf{x}) < 0\}.$$

This boundary condition (2.4) guarantees the global conservation of mass for any accommodation coefficient $\alpha \in [0,1]$ [4]. Moreover, in the specular case $\alpha = 0$ the energy of f is globally conserved [9].

Therefore, for hydrodynamics quantities $(\rho, \rho\mathbf{u}, E)$, the specular reflection applied at the kinetic level, implies slip boundary conditions [4,9], which correspond to a zero-flux boundary condition for the mean velocity:

$$\mathbf{u}\cdot\mathbf{n} = 0.$$

This condition yields in particular the global conservation of mass and kinetic energy. Moreover, pure diffuse boundary conditions ($\alpha = 1$) impose also a zero-flux boundary condition for the mean velocity. This yields the global conservation of mass at the macroscopic level.

The main issue for the numerical discretization of these boundary conditions relies on that the inflow is no longer a given function, while it is determined by the outflow. For this, we proceed in three steps: we first compute the outflow at the ghost points. To maintain high order accuracy and to prevent spurious oscillations caused by shocks, we use a weighted essentially non-oscillatory (WENO) type extrapolation to approximate the ghost points using the values of interior mesh points. In the same time, we can extrapolate the outflow located at the boundary associated with ghost points. Then, we compute the inflow at the boundary using the outflow obtained in the first step and the Maxwell's boundary conditions. Finally, we perform the inverse Lax–Wendroff procedure to approximate the inflow on the ghost points, where the key point is to replace the normal derivatives by a reformulation of the original kinetic equation.

In this paper we only apply a second order finite difference method to discretize the transport term of (2.1), but other numerical schemes may be used like WENO or ENO schemes [13] or semi-Lagrangian schemes [5]. Concerning boundary conditions, we will also restrict ourselves to second order approximation. Indeed, we will see that higher order methods would require additional evaluations of the collision operator which can be costly. However, let us emphasize that the second order inverse Lax–Wendroff method can be extended to higher order using WENO extrapolation [22]. Then to keep the order of accuracy of the method, two ghost points should be added in each direction in space. To impose f at the ghost points, we will apply the inverse Lax–Wendroff procedure proposed in [21] for conservation laws.

Suppose that the distribution function f at time level t^n for all interior points is already known, we now construct f at the ghost points.

2.1. One-dimensional case

We start with a one-dimensional space problem, that is $d_{\mathbf{x}} = 1$. In this case the Boltzmann equation reads:

$$\frac{\partial f}{\partial t} + v_x\frac{\partial f}{\partial x} = \frac{1}{\varepsilon}\mathcal{Q}(f), \quad (x,\mathbf{v}) \in [x_l, x_r] \times \mathbb{R}^3, \tag{2.8}$$

where x_l and x_r are the left and right boundaries respectively, v_x is the component of velocity field corresponding to x-direction. For the boundary conditions in one-dimensional case, the inward normal on the boundary in (2.4) is

$$\mathbf{n}(x_l) = \begin{pmatrix} 1 \\ 0 \\ 0 \end{pmatrix}, \quad \mathbf{n}(x_r) = \begin{pmatrix} -1 \\ 0 \\ 0 \end{pmatrix}.$$

To implement the numerical method, we assume the computational domain is a bounded domain $[x_{\min}, x_{\max}] \times [-V, V]^3$, where $(x_l, x_r) \subset [x_{\min}, x_{\max}]$. The computational domain is covered by a uniform Cartesian mesh $\mathbf{X}_h \times \mathbf{V}_h$,

$$\begin{cases} \mathbf{X}_h = \{x_{\min} = x_0 \leqslant \cdots \leqslant x_i \leqslant \cdots \leqslant x_{n_x} = x_{\max}\}, \\ \mathbf{V}_h = \{\mathbf{v}_j = j\Delta v,\ j = (j_1, j_2, j_3) \in \mathbb{Z}^3,\ |j| \leqslant n_v\}, \end{cases} \tag{2.9}$$

with the mesh size Δx and Δv for space and velocity respectively. We only describe the numerical calculation of ghost points near the left boundary, since the procedure for the right boundary is the same. Fig. 2 illustrates a portion of the mesh near the left boundary x_l, which is located between x_0 and x_1.

We denote $h = (\Delta x, \Delta v)$ and construct an approximation f_h of the distribution function at each ghost point following three steps: we perform an extrapolation f_h to compute a high order approximation of the outflow, *i.e.* $f_h(x_g, \mathbf{v}_{j^*}),\ x_g = x_0$ and x_{-1}. Then, we compute an approximation of the distribution function at the boundary using the Maxwell's boundary conditions. Finally, we apply the inverse Lax–Wendroff procedure for the inflow, *i.e.* $f_h(x_g, \mathbf{v}_j),\ x_g = x_0$ and x_{-1}.

2.1.1. First step: extrapolation f_h for the outflow

At time $t = t^n$ we consider the outflow near the point x_l, that is the values $f(t, x_l, \mathbf{v}_j)$ where $v_{j_1} < 0$. We denote by $f_{i,j}$ an approximation of f at $(x_i, \mathbf{v}_j)$.

A natural idea is to extrapolate f_h at the left boundary x_l and the ghost points x_0 and x_{-1} using the values on interior points. For example from the values $f_{1,j}, f_{2,j}$ and $f_{3,j}$, we can construct a Lagrange polynomial $p_2(x) \in \mathbb{P}_2(\mathbb{R})$. Then by injecting $x_l,\ x_0$ and x_{-1} into $p_2(x)$, we obtain the approximations f_h at the ghost points and the left boundary, *i.e.* $f_{l,j},\ f_{0,j}$ and $f_{-1,j}$. However, when a shock goes out of the boundary, the high order extrapolation may lead to a severe oscillation near the shock. To prevent this, we would like to have a lower order accurate but more robust extrapolation. Therefore, a WENO type extrapolation [21] will be applied and described below (see subSection 2.3) for this purpose.

2.1.2. Second step: compute boundary conditions

In the previous step, the outflow at the boundary is obtained by extrapolation. To compute the values of f at the inflow boundary, we apply the Maxwell's boundary conditions (2.4), i.e.

$$f_{l,j} = (1 - \alpha)\, \mathcal{R}[f_{l,j}] + \alpha\, \mathcal{M}[f_{l,j}]. \tag{2.10}$$

On the one hand the specular reflection portion is given by the outflow at the left boundary, which is

$$\mathcal{R}[f_{l,j}] = f_{l,j^\star}, \quad \text{where} \quad j^\star = (-j_1, j_2, j_3).$$

On the other hand the diffuse one is computed by a half Maxwellian

$$\mathcal{M}[f_{l,j}] = \mu_l \exp\left(-\frac{|\mathbf{v}_j|^2}{2T_l}\right),$$

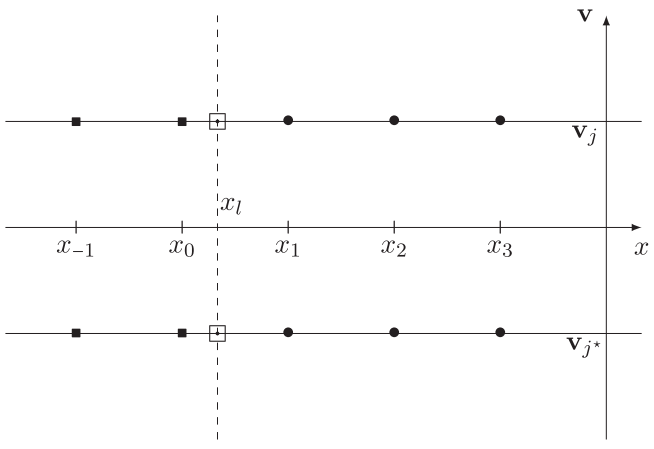

Fig. 2. A portion of the mesh in one dimensional case. • is interior point, ■ is ghost point, ⊡ is the left boundary.

where T_l is the given temperature at the left wall and μ_l is given by

$$\mu_l \sum_{\mathbf{v}_j\cdot\mathbf{n}(x_l)\geqslant 0} \mathbf{v}_j\cdot\mathbf{n}(x_l)\,\exp\left(-\frac{|\mathbf{v}_j|^2}{2T_l}\right) = -\sum_{\mathbf{v}_j\cdot\mathbf{n}(x_l)\leqslant 0} \mathbf{v}_j\cdot\mathbf{n}(x_l) f_{l,j}.$$

2.1.3. Third step: approximation f_h for the inflow

Finally we compute the values of f_h at the ghost points for the inflow. Here we cannot approximate f_h by an extrapolation, since the distribution function at interior points cannot predict the inflow. Thus we extend the inverse Lax–Wendroff type procedure recently proposed in [11,21,24] for conservation laws. At the left boundary x_l, a first order Taylor expansion gives

$$f_h(x,v_j) = f_{l,j} + (x-x_l)\left.\frac{\partial f_h}{\partial x}\right|_{(x,v)=(x_l,v_j)} + O(\Delta x^2).$$

Hence a second order approximation of f at ghost points is

$$f_{s,j} = f_{l,j} + (x_s-x_l)\left.\frac{\partial f_h}{\partial x}\right|_{(x,v)=(x_l,v_j)}, \quad s=-1,0. \tag{2.11}$$

We already computed $f_{l,j}$ in the second step, thus it remains to obtain an approximation of the first derivative. By reformulating (2.8), we have

$$\left.\frac{\partial f_h}{\partial x}\right|_{x=x_l} = \frac{1}{v_x}\left(-\frac{\partial f_h}{\partial t} + \frac{1}{\varepsilon}\mathcal{Q}(f_h)\right)\Big|_{x=x_l}. \tag{2.12}$$

Now instead of approximating the first derivative $\partial_x f|_{x=x_l}$, we compute an approximation of the time derivative $\partial_t f|_{x=x_l}$ and the collision operator $\mathcal{Q}(f)|_{x=x_l}$. An approximation of the time derivative can be computed using several $f_{l,j}$ at previous time levels. Different approximations can be obtained. At first order one could use

$$\left.\frac{\partial f_h}{\partial t}\right|_{x=x_l} \simeq \frac{f_{l,j}^n - f_{l,j}^{n-1}}{\Delta t},$$

where Δt is the time step. For higher order one can use a WENO type extrapolation to approximate the time derivative (see Section 2.3 below).

The last term $\mathcal{Q}(f_h)|_{x=x_l}$ can be computed explicitly using $f_{l,j}$ obtained in previous two steps. Clearly this procedure is independent of the values of f at interior points.

Remark 2.1. Let us address the following points to increase the order of accuracy and to stabilize the inverse Lax–Wendroff procedure.

1. Here, we restrict our presentation to a second order accurate method, since the higher order ILW procedure becomes more complicated to apply (it would require several evaluations of the collision operator). To achieve higher order accuracy, we can follow the ideas in [22], where the second order derivative can be approximated using a WENO type extrapolation from the interior points.
2. Let us notice that when $v_x \to 0$ or when $\varepsilon \to 0$ at the boundary, the formula (2.12) gives an approximation $\partial_x f_h^{ILW}(x_l, v_j)$, which may blow-up and the inverse Lax–Wendroff procedure may generate spurious oscillations. Therefore, a limitation procedure based on the WENO extrapolation is applied. For instance, at the boundary point x_l, the second step gives values $(f_{l,j})_j$, then using interior points we construct a WENO polynomial interpolation and compute approximated values $f_{1^*,j}$ at point $x_l + \Delta x$ and $f_{2^*,j}$ at point $x_l + 2\Delta x$. Hence from these later points, we compute a WENO type extrapolation a new approximation of the first derivative denoted by $\partial_x f_h^{WENO}(x_l, v_j)$. Finally, we introduce an approximation $\partial_x f_h(x_l, v_j)$ by

$$\partial_x f_h(x_l, v_j) = \operatorname{minmod}\left(\partial_x f_h^{ILW}, \partial_x f_h^{WENO}\right)(x_l, v_j). \tag{2.13}$$

This procedure prevents spurious oscillations and numerical instabilities of the inverse Lax–Wendroff procedure.
3. Let us observe that when $\alpha = 0$ we have a pure specular reflection condition. A mirror procedure can be used to approximate f at the ghost points. More precisely, by considering the boundary as a mirror, we approximate the distribution at the ghost points $f(x_s, v_j)$ as

$$f(x_s, \mathbf{v}_j) = f(2x_l - x_s, \mathbf{v}_{j^\star}), \quad \text{where} \quad j^\star = (-j_1, j_2, j_3),$$

where $2x_l - x_s$ is the mirror image point of x_s. Since $2x_l - x_s$ is located in interior domain, we can approximate $f(2x_l - x_s, \mathbf{v}_{j^\star})$ by an interpolation procedure.

2.2. Two-dimensional case

The previous approach can be generalized to two-dimensional problems. We assume $d_{\mathbf{x}} = 2$ in Eq. (2.1)

$$\frac{\partial f}{\partial t} + v_x \frac{\partial f}{\partial x} + v_y \frac{\partial f}{\partial y} = \frac{1}{\varepsilon} Q(f), \tag{2.14}$$

where the distribution function $f(t, \mathbf{x}, \mathbf{v})$ is defined in $(t, \mathbf{x}, \mathbf{v}) \in \mathbb{R}^+ \times \Omega \times \mathbb{R}^3$ with $\mathbf{x} = (x, y)$. We consider a computational domain $[x_{\min}, x_{\max}] \times [y_{\min}, y_{\max}] \times [-V, V]^3$, such that $\Omega \subset [x_{\min}, x_{\max}] \times [y_{\min}, y_{\max}]$ and $f(t, \mathbf{x}, \mathbf{v}) \approx 0$, for all $\|\mathbf{v}\| \geqslant V$.

The computational domain is covered by an uniform Cartesian mesh $\mathbf{X}_h \times \mathbf{V}_h$, where $\mathbf{X}_h$, $\mathbf{V}_h$ are defined similarly to (2.9). The mesh steps are respectively Δx, Δy and Δv. In Fig. 3, we present a portion of the mesh in space near the boundary. From a ghost point $\mathbf{x}_g$, we can find an inward normal $\mathbf{n}$, which crosses the boundary at $\mathbf{x}_p$.

For the 2D case, the numerical approximation of the distribution function f at ghost points is similar to the one dimensional case. However, there are two major differences. First to compute $\mathcal{R}[f]$ in the second step, the corresponding reflected velocities may not correspond to grid nodes in phase space. Secondly to approximate the normal derivative in the third step, besides the time derivative and collision operator we need also the tangential derivative at $\mathbf{x}_p$. Once again, we present the method in three steps:

2.2.1. First step: extrapolation of f for the outflow

Let us assume that the values of the distribution function f on the grid points in Ω are given. To approximate f at a ghost point, for instance $\mathbf{x}_g$, we first construct a stencil $\mathcal{E}$ composed of grid points of Ω for the extrapolation. For instance as it is shown in Fig. 3, the inward normal $\mathbf{n}$ intersects the grid lines $y = y_{i_y}, y_{i_y+1}, y_{i_y+2}$ at points P_0^*, P_1^*, P_2^*. Then we choose the three nearest points of the cross point P_l^*, $l = 0, 1, 2$, in each line, *i.e.* marked by a large circle. From these nine points, we can build a Lagrange polynomial $q_2(\mathbf{x}) \in \mathbb{Q}_2(\mathbb{R}^2)$. Therefore we evaluate the polynomial $q_2(\mathbf{x})$ at $\mathbf{x}_g$ and $\mathbf{x}_p$, and obtain an approximation of f at the boundary and at ghost points. As for the 1D case, a WENO type extrapolation can be used to prevent spurious oscillations, which will be detailed in subSection 2.3.

Note that in some cases, we cannot find a stencil of nine interior points. For instance when the interior domain has a small acute angle sharp, the normal $\mathbf{n}$ cannot have three cross points P_l^*, $l = 0, 1, 2$ in interior domain, or we cannot have three nearest points of the cross point P_l^*, $l = 0, 1, 2$, in each line. In such a case, we alternatively use a first degree polynomial $q_1(\mathbf{x})$ with a four points stencil or even a zero degree polynomial $q_0(\mathbf{x})$ with a one point stencil. We can similarly construct the four points stencil or the one point stencil as above.

2.2.2. Second step: compute boundary conditions

In the previous step, we have obtained the outflow $f(\mathbf{x}_p, \mathbf{v} \cdot \mathbf{n} < 0)$ at the boundary $\mathbf{x}_p$. Using (2.4) as we did for the 1D case, we can similarly compute the distribution function f for $\mathbf{v} \cdot \mathbf{n} \geqslant 0$. However now the distribution function for specular reflection is given by

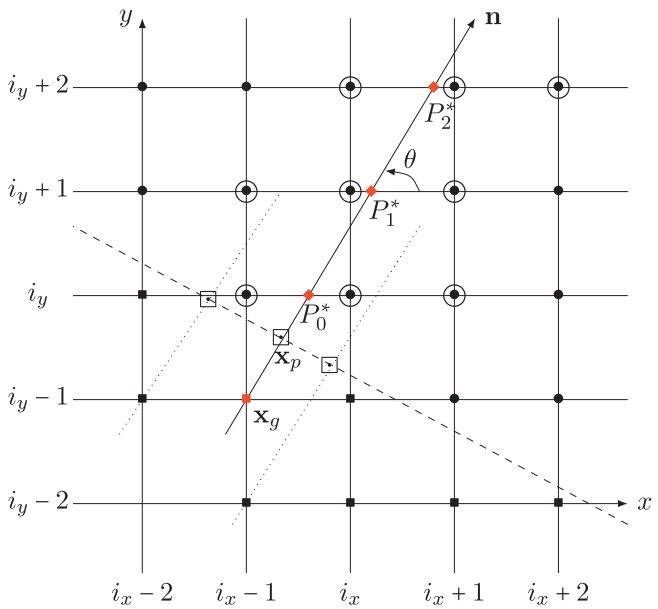

Fig. 3. Two-dimensional Cartesian mesh. • is interior point, ■ is ghost point, ⊡ is the point at the boundary, ∘ is the point for extrapolation, the dashed line is the boundary.

$$\mathcal{R}[f(\mathbf{x}_p,\mathbf{v})] = f(\mathbf{x}_p,\mathbf{v}-2(\mathbf{v}\cdot\mathbf{n})\mathbf{n}), \quad \forall \mathbf{v}\in\mathbf{V}_h$$

and the vector fields $\mathbf{v}-2(\mathbf{v}\cdot\mathbf{n})\mathbf{n}$ may not be located on a grid point. Therefore, we interpolate f in phase space $(\mathbf{x}_p,\mathbf{v}-2(\mathbf{v}\cdot\mathbf{n})\mathbf{n})$ using the values computed from the outflow $f(\mathbf{x}_p,\mathbf{v})$ such that $\mathbf{v}\cdot\mathbf{n}\geqslant 0$.

2.2.3. Third step: approximation of f for the inflow

We have obtained the values of f at the boundary points $\mathbf{x}_p$ for all $\mathbf{v}\in\mathbf{V}_h$ in previous two steps. Now we reconstruct the values of f for the velocity grid points such that $\mathbf{v}\cdot\mathbf{n}\geqslant 0$ at the ghost point $\mathbf{x}_g$ by a simple Taylor expansion in the inward normal direction. To this end, we set up a local coordinate system at $\mathbf{x}_p$ by

$$\hat{\mathbf{x}} = \begin{pmatrix}\hat{x}\\ \hat{y}\end{pmatrix} = \begin{pmatrix}\cos\theta & \sin\theta\\ -\sin\theta & \cos\theta\end{pmatrix}\begin{pmatrix}x\\ y\end{pmatrix},$$

where θ is the angle between the inward normal $\mathbf{n}$ and the x-axis illustrated in Fig. 3. Thus the first order approximation of $f(\mathbf{x}_g,\mathbf{v})$ reads

$$f(\mathbf{x}_g,\mathbf{v})\approx\hat{f}(\hat{\mathbf{x}}_p,\mathbf{v}) + (\hat{x}_g-\hat{x}_p)\frac{\partial\hat{f}}{\partial\hat{x}}(\hat{\mathbf{x}}_p,\mathbf{v}),$$

where $\hat{f}(\hat{\mathbf{x}}_p,\mathbf{v}) = f(\mathbf{x}_p,\mathbf{v})$ and $\frac{\partial\hat{f}}{\partial\hat{x}}(\hat{\mathbf{x}}_p,\mathbf{v})$ is the first order normal derivative at the boundary $\mathbf{x}_p$. To approximate $\frac{\partial\hat{f}}{\partial\hat{x}}(\hat{\mathbf{x}}_p,\mathbf{v})$, we use inverse Lax–Wendroff procedure. Firstly, we rewrite the Eq. (2.14) in the local coordinate system as

$$\frac{\partial\hat{f}}{\partial t} + \hat{v}_x\frac{\partial\hat{f}}{\partial\hat{x}} + \hat{v}_y\frac{\partial\hat{f}}{\partial\hat{y}} = \frac{1}{\varepsilon}\mathcal{Q}(\hat{f}), \tag{2.15}$$

where $\hat{v}_x = v_x\cos\theta + v_y\sin\theta,\ \hat{v}_y = -v_x\sin\theta + v_y\cos\theta$. Then a reformulation of (2.15) yields

$$\frac{\partial\hat{f}}{\partial\hat{x}}(\hat{\mathbf{x}}_p,\mathbf{v}) = -\frac{1}{\hat{v}_x}\left(\frac{\partial\hat{f}}{\partial t} + \hat{v}_y\frac{\partial\hat{f}}{\partial\hat{y}} - \frac{1}{\varepsilon}\mathcal{Q}(\hat{f})\right)\Bigg|_{\hat{\mathbf{x}}=\hat{\mathbf{x}}_p}. \tag{2.16}$$

Finally instead of approximating $\frac{\partial\hat{f}}{\partial\hat{x}}(\hat{\mathbf{x}}_p,\mathbf{v})$ directly, we approximate the time derivative $\frac{\partial\hat{f}}{\partial t}$, the tangential derivative $\frac{\partial\hat{f}}{\partial\hat{y}}$ and the collision operator $\mathcal{Q}(\hat{f})$. Similarly as in one-dimensional case, we compute $\frac{\partial\hat{f}}{\partial t}$ and $\mathcal{Q}(\hat{f})$, but it remains to approximate $\frac{\partial\hat{f}}{\partial\hat{y}}$.

When the boundary is a straight line, we can use some neighbor points of $\mathbf{x}_p$ at the boundary to approximate the tangential derivative $\frac{\partial\hat{f}}{\partial\hat{y}}$. However, when the boundary is a curve, we cannot use the neighbor points to approximate $\frac{\partial\hat{f}}{\partial\hat{y}}$. Here we approximate the tangential derivative using interior points. Precisely, we define $h = \min(\Delta x,\Delta y)$ and space step $\hat{h}_y = (0,h)$ in local coordinates $(\hat{x},\hat{y})$. Then the tangential derivative $\frac{\partial\hat{f}}{\partial\hat{y}}$ can be calculated by an ENO type approximation as follows

$$\frac{\partial\hat{f}}{\partial\hat{y}}(\hat{\mathbf{x}},\mathbf{v}) = \operatorname{minmod}\left(\frac{f(\hat{\mathbf{x}}+\hat{h}_y,\mathbf{v})-f(\hat{\mathbf{x}},\mathbf{v})}{h}, \frac{f(\hat{\mathbf{x}},\mathbf{v})-f(\hat{\mathbf{x}}-\hat{h}_y,\mathbf{v})}{h}\right), \quad \mathbf{n}\cdot\mathbf{v}\geqslant 0,$$

where $f(\hat{\mathbf{x}}+\hat{h}_y,\mathbf{v})$ and $f(\hat{\mathbf{x}}-\hat{h}_y,\mathbf{v})$ can be obtained by an interpolation in concave boundary case, or by a WENO type extrapolation in convex boundary case.

Remark 2.2. As in one dimensional case, when $\hat{v}_x$ is small or when ε goes to zero at the boundary, the formula (2.16) blows up and the inverse Lax–Wendroff procedure is not appropriate. Therefore a WENO type extrapolation is applied using interior points. More precisely, we first interpolate f at points $\mathbf{x}+\hat{h}_x$ and $\mathbf{x}+2\hat{h}_x$, where $\hat{h}_x = (h,0)$, *i.e.* $\hat{f}(\hat{\mathbf{x}}_p+\hat{h}_x,\mathbf{v}),\hat{f}(\hat{\mathbf{x}}_p+2\hat{h}_x,\mathbf{v}),\mathbf{n}\cdot\mathbf{v}\geqslant 0$. We then extrapolate $f(\mathbf{x}_g,\mathbf{v})$ with the WENO type extrapolation using $\hat{f}(\hat{\mathbf{x}}_p,\mathbf{v}),\hat{f}(\hat{\mathbf{x}}_p+\hat{h}_x,\mathbf{v})$ and $\hat{f}(\hat{\mathbf{x}}_p+2\hat{h}_x,\mathbf{v})$.

2.3. WENO type extrapolation

A WENO type extrapolation [21] was developed to prevent oscillations and maintain accuracy, which is an extension of WENO scheme [13]. The key point of WENO type extrapolation is to define smoothness indicators, which is designed to help us choose automatically between the high order accuracy and the low order but more robust extrapolation. Here we describe this method in 1D and 2D cases. Moreover we will give a slightly modified version of the method such that the smoothness indicators are invariant with respect to the scaling of f.

2.3.1. One-dimensional WENO type extrapolation

Assume that we have a stencil of three points $\mathcal{E} = \{x_1,x_2,x_3\}$ showed in Fig. 2 and denote the corresponding distribution function by $f_1,\ f_2,\ f_3$. Instead of extrapolating f at ghost point x_g by Lagrange polynomial, we use following Taylor expansion

$$f_g = \sum_{k=0}^{2} \frac{(x_g - x_l)^2}{k!} \frac{d^k f}{dx^k}\bigg|_{x=x_l}.$$

We aim to obtain a $(3-k)$th order approximation of $\frac{d^k f}{dx^k}\big|_{x=x_l}$ denoted by $f_l^{(k)},\ k=0,1,2$. Three candidate substencils are given by

$$S_r = \{x_1, \ldots, x_{r+1}\}, \quad r = 0,1,2.$$

In each substencil S_r, we could construct a Lagrange polynomial $p_r(x) \in \mathbb{P}_r(\mathbb{R})$

$$\begin{cases} p_0(x) = f_1, \\ p_1(x) = f_1 + \frac{f_2 - f_1}{\Delta x}(x - x_1), \\ p_2(x) = f_1 + \frac{f_2 - f_1}{\Delta x}(x - x_1) + \frac{f_3 - 2f_2 + f_1}{2\Delta x^2}(x - x_1)(x - x_2). \end{cases}$$

We now look for the WENO type extrapolation in the form

$$f_l^{(k)} = \sum_{r=0}^{2} w_r \frac{d^k p_r(x)}{dx^k}(x_l),$$

where w_r are the nonlinear weights depending on f_i. We expect that $f_l^{(k)}$ has $(3-k)$-order accurate in the case $f(x)$ is smooth in S_2. The nonlinear weights are given by

$$w_r = \frac{\alpha_r}{\sum_{s=0}^{2} \alpha_s},$$

with

$$\alpha_r = \frac{d_r}{(\varepsilon + \beta_r)^2},$$

where $\varepsilon = 10^{-6},\ d_0 = \Delta x^2,\ d_1 = \Delta x,\ d_2 = 1 - \Delta x - \Delta x^2$ and β_r are the new smoothness indicators determined by $\beta_0 = \Delta x^2$, then if $(f_1, f_2) = (0,0)$, we take $\beta_1 = 0$ else we choose

$$\beta_1 = \frac{1}{f_1^2 + f_2^2} \sum_{l=1}^{2} \int_{x_0}^{x_1} \Delta x^{2l-1} \left(\frac{d^l}{dx^l} p_1(x) \right)^2 dx = \frac{(f_2 - f_1)^2}{f_1^2 + f_2^2}$$

and finally if $(f_1, f_2, f_3) = (0,0,0)$, we take $\beta_2 = 0$ else, we choose

$$\beta_2 = \frac{1}{f_1^2 + f_2^2 + f_3^2} \sum_{l=1}^{2} \int_{x_0}^{x_1} \Delta x^{2l-1} \left(\frac{d^l}{dx^l} p_2(x) \right)^2 dx = \frac{1}{12(f_1^2 + f_2^2 + f_3^2)} (61 f_1^2 + 160 f_2^2 + 25 f_3^2 + 74 f_1 f_3 - 192 f_1 f_2 - 124 f_2 f_3).$$

We remark that the smoothness indicators β_1 and β_2 have the factors $\frac{1}{\sum_{m=1}^{r+1} f_m^2}$, which guarantee that the indicators are invariant of the scaling of f_i.

2.3.2. Two-dimensional extrapolation

The two-dimensional extrapolation is a straightforward expansion of the 1D case. The substencils $S_r,\ r = 0,1,2$ for extrapolation are chosen around the inward normal $\mathbf{n}$ such that we can construct Lagrange polynomial of degree r. For instance in Fig. 3, the three substencils are respectively

$$\begin{cases} S_0 = \{(x_{i_x}, y_{i_y})\}, \\ S_1 = \{(x_{i_x-1}, y_{i_y}), (x_{i_x}, y_{i_y}), (x_{i_x}, y_{i_y+1}), (x_{i_x+1}, y_{i_y+1})\}, \\ S_2 = \{(x_{i_x-1}, y_{i_y}), (x_{i_x}, y_{i_y}), (x_{i_x+1}, y_{i_y}), (x_{i_x-1}, y_{i_y+1}), \\ \qquad (x_{i_x}, y_{i_y+1}), (x_{i_x+1}, y_{i_y+1}), (x_{i_x}, y_{i_y+2}), (x_{i_x+1}, y_{i_y+2}), (x_{i_x+2}, y_{i_y+2})\}. \end{cases}$$

Once the substencils S_r are chosen, we could easily construct the Lagrange polynomials in $\mathbb{Q}_r(\mathbb{R}^2)$

$$q_r(\mathbf{x}) = \sum_{m=0}^{r} \sum_{l=0}^{r} a_{l,m} x^l y^m$$

satisfying

$$q_r(\mathbf{x}) = f(\mathbf{x}), \quad \mathbf{x} \in S_r.$$

Then the WENO extrapolation has the form

$$f(\mathbf{x}) = \sum_{r=0}^{2} w_r q_r(\mathbf{x}), \quad \mathbf{x} \in S_r, \tag{2.17}$$

where w_r are the nonlinear weights, which are chosen to be

$$w_r = \frac{\alpha_r}{\sum_{s=0}^{2} \alpha_s},$$

with

$$\alpha_r = \frac{d_r}{(\varepsilon + \beta_r)^2},$$

where $\varepsilon = 10^{-6},\ d_0 = \Delta x^2 + \Delta y^2,\ d_1 = \sqrt{\Delta x^2 + \Delta y^2},\ d_2 = 1 - d_0 - d_1$. β_r are the smoothness indicators determined by

$$\beta_0 = \Delta x^2 + \Delta y^2,$$

and if $f(\mathbf{x}) = 0,\ \forall \mathbf{x} \in S_r$ we take $\beta_r = 0$, else

$$\beta_r = \frac{1}{\sum_{\mathbf{x} \in S_r} f(\mathbf{x})^2} \sum_{1 \leqslant |\sigma| \leqslant r} \int_K |K|^{|\sigma|-1} (D^\sigma q_r(\mathbf{x}))^2 d\mathbf{x}, \quad r = 1, 2,$$

where σ is a multi-index and $K = [x_p - \Delta x/2, x_p + \Delta x/2] \times [y_p - \Delta y/2, y_p + \Delta y/2], \mathbf{x}_p = (x_p, y_p)$.

3. Application to the ES-BGK model

The Boltzmann equation (2.1) governs well the evolution of the density f in kinetic regime and also in the continuum regime [4]. However the quadratic collision operator $\mathcal{Q}(f)$ has a rather complex form such that it is very difficult to compute. Hence different simpler models have been introduced. The simplest model is the so-called BGK model [3], which is mainly a relaxation towards a Maxwellian equilibrium state

$$\mathcal{Q}(f) = \frac{\tau}{\varepsilon}(\mathcal{M}[f] - f), \tag{3.1}$$

where $\tau = \pi\rho$.

Although it describes the correct hydrodynamic limit, the BGK model does not give the Navier–Stokes equation with correct transport coefficients in the Chapman–Enskog expansion. Holway *et al.* [10] proposed the ES-BGK model, where the Maxwellian $\mathcal{M}[f]$ in the relaxation term of (3.1) is replaced by an anisotropic Gaussian $\mathcal{G}[f]$. This model has correct conservation laws, yields the Navier-Stokes approximation via the Chapman-Enskog expansion with a Prandtl number less than one, and yet is endowed with the entropy condition [1]. In order to introduce the Gaussian model, we need further notations. Define the opposite of the stress tensor

$$\Theta(t, \mathbf{x}) = \frac{1}{\rho} \int_{\mathbb{R}^3} (\mathbf{v} - \mathbf{u}) \otimes (\mathbf{v} - \mathbf{u}) f(t, \mathbf{x}, \mathbf{v}) d\mathbf{v}. \tag{3.2}$$

Therefore the translational temperature is related to the $T = \mathrm{tr}(\Theta)/3$. We finally introduce the corrected tensor

$$\mathcal{T}(t, \mathbf{x}) = [(1 - v)T\mathrm{I} + v\Theta](t, \mathbf{x}),$$

which can be viewed as a linear combination of the initial stress tensor Θ and of the isotropic stress tensor $T\mathrm{I}$ developed by a Maxwellian distribution, where I is the identity matrix.

The ES-BGK model introduces a corrected BGK collision operator by replacing the local equilibrium Maxwellian by the Gaussian $\mathcal{G}[f]$ defined by

$$\mathcal{G}[f] = \frac{\rho}{\sqrt{\det(2\pi\mathcal{T})}} \exp\left(-\frac{(\mathbf{v} - \mathbf{u})\mathcal{T}^{-1}(\mathbf{v} - \mathbf{u})}{2}\right).$$

Thus, the corresponding collision operator is now

$$\mathcal{Q}(f) = \frac{\tau}{\varepsilon}(\mathcal{G}[f] - f), \tag{3.3}$$

where $\tau = \pi\rho$, the parameter $-1/2 \leqslant v < 1$ is used to modify the value of the Prandtl number through the formula

$$\frac{2}{3} \leqslant \mathrm{Pr} = \frac{1}{1 - v} \leqslant +\infty.$$

It follows from the above definitions that

$$\begin{cases} \int_{\mathbb{R}^3} f(\mathbf{v})\, d\mathbf{v} = \int_{\mathbb{R}^3} \mathcal{G}[f](\mathbf{v})\, d\mathbf{v} = \rho, \\ \int_{\mathbb{R}^3} \mathbf{v} f(\mathbf{v})\, d\mathbf{v} = \int_{\mathbb{R}^3} \mathbf{v}\, \mathcal{G}[f](\mathbf{v})\, d\mathbf{v} = \rho\mathbf{u}, \\ \int_{\mathbb{R}^3} \frac{|\mathbf{v}|^2}{2} f(\mathbf{v})\, d\mathbf{v} = \int_{\mathbb{R}^3} \frac{|\mathbf{v}|^2}{2} \mathcal{G}[f](\mathbf{v})\, d\mathbf{v} = E \end{cases} \tag{3.4}$$

and

$$\begin{cases} \int_{\mathbb{R}^3} (\mathbf{v}-\mathbf{u}) \otimes (\mathbf{v}-\mathbf{u}) f(\mathbf{v})\, d\mathbf{v} = \rho\,\Theta, \\ \int_{\mathbb{R}^3} (\mathbf{v}-\mathbf{u}) \otimes (\mathbf{v}-\mathbf{u})\, \mathcal{G}[f]\, d\mathbf{v} = \rho\,\mathcal{T}. \end{cases}$$

This implies that this collision operator does indeed conserve mass, momentum and energy as imposed.

In this section, we will first recall the implicit-explicit (IMEX) scheme to the ES-BGK equation proposed in [3]. Then we apply our ILW procedure to treat boundary conditions for the ES-BGK model.

3.1. An IMEX scheme to the ES-BGK equation

We now introduce the time discretization for the ES-BGK equations (2.1) and (3.3)

$$\begin{cases} \frac{\partial f}{\partial t} + \mathbf{v}\cdot\nabla_{\mathbf{x}} f = \frac{\tau}{\varepsilon}(\mathcal{G}[f] - f), \quad \mathbf{x}\in\Omega\subset\mathbb{R}^{d_{\mathbf{x}}},\ \mathbf{v}\in\mathbb{R}^3, \\ f(0,\mathbf{x},\mathbf{v}) = f_0(\mathbf{x},\mathbf{v}), \quad \mathbf{x}\in\Omega,\ \mathbf{v}\in\mathbb{R}^3, \end{cases} \tag{3.5}$$

where $\tau = \pi\rho$.

The time discretization is an IMEX scheme. Since the convection term in (3.5) is not stiff, we will treat it explicitly. The source terms on the right hand side of (3.5) will be handled using an implicit solver. We simply apply a first order IMEX scheme,

$$\begin{cases} \frac{f^{n+1}-f^n}{\Delta t} + \mathbf{v}\cdot\nabla_{\mathbf{x}} f^n = \frac{\tau^{n+1}}{\varepsilon}(\mathcal{G}[f^{n+1}] - f^{n+1}), \\ f^0(\mathbf{x},\mathbf{v}) = f_0(\mathbf{x},\mathbf{v}). \end{cases} \tag{3.6}$$

This can be written as

$$f^{n+1} = \frac{\varepsilon}{\varepsilon+\tau^{n+1}\Delta t}[f^n - \Delta t\,\mathbf{v}\cdot\nabla_{\mathbf{x}} f^n] + \frac{\tau^{n+1}\Delta t}{\varepsilon+\tau^{n+1}\Delta t}\,\mathcal{G}[f^{n+1}], \tag{3.7}$$

where $\mathcal{G}(f^{n+1})$ is the anisotropic Maxwellian distribution computed from f^{n+1}. Although (3.7) appears nonlinearly implicit, since the computation of f^{n+1} requires the knowledge of $\mathcal{G}[f^{n+1}]$, it can be solved explicitly. Specifically, upon multiplying (3.7) by $\phi(\mathbf{v})$ defined by

$$\phi(\mathbf{v}) := \left(1, \mathbf{v}, \frac{|\mathbf{v}|^2}{2}\right)$$

and use the conservation properties of $\mathcal{Q}$ and the definition of $\mathcal{G}[f]$ in (2.3), we define the macroscopic quantity U by $U := (\rho, \rho\,\mathbf{u}, E)$ computed from f and get

$$U^{n+1} = \frac{\varepsilon}{\varepsilon+\tau^{n+1}\Delta t}\int_{\mathbb{R}^3}\phi(\mathbf{v})\,(f^n - \Delta t\,\mathbf{v}\cdot\nabla_{\mathbf{x}} f^n)\,d\mathbf{v} + \frac{\tau^{n+1}\Delta t}{\varepsilon+\tau^{n+1}\Delta t}\int_{\mathbb{R}^3}\phi(\mathbf{v})\mathcal{G}[f^{n+1}](\mathbf{v})\,d\mathbf{v}$$

or simply

$$U^{n+1} = \int_{\mathbb{R}^3}\phi(\mathbf{v})\,(f^n - \Delta t\mathbf{v}\cdot\nabla_{\mathbf{x}} f^n)\,d\mathbf{v}. \tag{3.8}$$

Thus U^{n+1} can be obtained explicitly. This gives ρ^{n+1}, $\mathbf{u}^{n+1}$ and T^{n+1}. Until now the IMEX scheme is the same as the IMEX scheme for BGK model proposed in [20]. Since the Maxwellian $\mathcal{M}(f)$ depends only macroscopic quantities, we can solve explicitly f^{n+1} for the BGK model. Unfortunately for the ES-BGK model, it is not enough to define $\mathcal{G}[f^{n+1}]$ for which we need $\rho^{n+1}\,\Theta^{n+1}$. Therefore, we define the tensor Σ by

$$\Sigma^{n+1} := \int_{\mathbb{R}^3}\mathbf{v}\otimes\mathbf{v} f^{n+1}\,d\mathbf{v} = \rho^{n+1}\left(\Theta^{n+1} + \mathbf{u}^{n+1}\otimes\mathbf{u}^{n+1}\right) \tag{3.9}$$

and multiply the scheme (3.7) by $\mathbf{v}\otimes\mathbf{v}$. Using the fact that

$$\int_{\mathbb{R}^3}\mathbf{v}\otimes\mathbf{v}\mathcal{G}[f](\mathbf{v})\,d\mathbf{v} = \rho\,(\mathcal{T} + \mathbf{u}\otimes\mathbf{u})$$

and (3.9), we get that

$$\Sigma^{n+1} = \frac{\varepsilon}{\varepsilon+(1-\nu)\,\tau^{n+1}\,\Delta t}\left(\Sigma^n - \Delta t\int_{\mathbb{R}^3}\mathbf{v}\otimes\mathbf{v}\,\mathbf{v}\cdot\nabla_{\mathbf{x}} f^n d\mathbf{v}\right) + \frac{(1-\nu)\,\tau^{n+1}\,\Delta t}{\varepsilon+(1-\nu)\,\tau^{n+1}\,\Delta t}\,\rho^{n+1}\left(T^{n+1}\,\mathrm{I} + \mathbf{u}^{n+1}\otimes\mathbf{u}^{n+1}\right). \tag{3.10}$$

Now $\mathcal{G}[f^{n+1}]$ can be obtained explicitly from U^{n+1} and Σ^{n+1} and then f^{n+1} from (3.7).

Finally the scheme reads

$$\begin{cases} U^{n+1} &= \int_{\mathbb{R}^3} \phi(\mathbf{v}) \left(f^n - \Delta t \mathbf{v}\cdot\nabla_{\mathbf{x}} f^n\right) d\mathbf{v}, \\ \Sigma^{n+1} &= \frac{\varepsilon}{\varepsilon+(1-\nu)\,\tau^{n+1}\,\Delta t}\left(\Sigma^n - \Delta t \int_{\mathbb{R}^3} \mathbf{v}\otimes\mathbf{v}\,\mathbf{v}\cdot\nabla_{\mathbf{x}} f^n d\mathbf{v}\right) \\ &\quad + \frac{(1-\nu)\,\tau^{n+1}\,\Delta t}{\varepsilon+(1-\nu)\,\tau^{n+1}\,\Delta t}\,\rho^{n+1}\left(T^{n+1}\,\mathrm{I} + \mathbf{u}^{n+1}\otimes\mathbf{u}^{n+1}\right), \\ f^{n+1} &= \frac{\varepsilon}{\varepsilon+\tau^{n+1}\Delta t}\left[f^n - \Delta t\,\mathbf{v}\cdot\nabla_{\mathbf{x}} f^n\right] + \frac{\tau^{n+1}\Delta t}{\varepsilon+\tau^{n+1}\Delta t}\,\mathcal{G}[f^{n+1}]. \end{cases} \tag{3.11}$$

The scheme (3.11) is an AP scheme for (3.6). On the one hand, although (3.6) is nonlinearly implicit, is can be solved explicitly. On the other hand, the scheme (3.11) preserves the correct asymptotic [8], which means when holding the mesh size and time step fixed and letting the Knudsen number go to zero, the scheme becomes a suitable scheme for the limiting hydrodynamic models.

Remark 3.1. To improve the numerical accuracy, second order schemes are sometimes more desirable. For this we will follow the IMEX scheme proposed by Filbet *et al.* [7]. Assume that an approximate solution f_n is known at time t_n , we compute a first approximation at time t^* using a first order IMEX scheme and next apply the trapezoidal rule and the midpoint formula. The scheme reads

$$\begin{cases} 2\frac{f^*-f^n}{\Delta t} + \mathbf{v}\cdot\nabla_{\mathbf{x}} f^n = \frac{\tau^*}{\varepsilon}(\mathcal{G}[f^*] - f^*), \\ \frac{f^{n+1}-f^n}{\Delta t} + \mathbf{v}\cdot\nabla_{\mathbf{x}} f^* = \frac{1}{2\varepsilon}(\tau^n(\mathcal{G}[f^n] - f^n) + \tau^{n+1}(\mathcal{G}[f^{n+1}] - f^{n+1})). \end{cases} \tag{3.12}$$

3.2. Inverse Lax–Wendroff procedure for boundary conditions

We have described the numerical method for boundary conditions to general kinetic equations in 1D and 2D case. To implement this method, it remains to replace the collision operator $\mathcal{Q}(f)$ in (2.12) or (2.16) by the ES-BGK operator (3.3).

Assume that the approximation to the distribution function at the boundary $f(\mathbf{x}_p, \mathbf{v})$ is known for all $\mathbf{v} \in \mathbf{V}_h$. Then, the macroscopic quantities $\rho, \mathbf{u}$ and T at the boundary point $\mathbf{x}_p$ can be obtained using (2.3) and (3.4). Therefore, substituting these macroscopic quantities in (3.2), we compute the stress tensor Θ at the boundary point $\mathbf{x}_p$, such that the corrected tensor $\mathcal{T}(\mathbf{x}_p)$. Thus $\mathcal{G}[f]$ is computed for all points $(\mathbf{x}_p, \mathbf{v})$, where $\mathbf{v} \in \mathbf{V}_h$.

4. Numerical examples

In this section, we present a large variety of test cases in $1d_x$ and $2d_x$ and three dimensional in velocity space showing the effectiveness of our method to get an accurate solution of Boltzmann type equations set in an arbitrary geometry with different boundary conditions. We perform a second order finite difference scheme for space discretization with Van Leer limiters [23] and the second order IMEX scheme presented in Remark 3.1. For the velocity discretization, the trapezoidal rules will be used.

We first give an example on a flow generated by gradients of temperature, which has already been treated by DSMC or other various methods [6]. Then, we present some numerical results in $2d_x$. The first one is a high-speed flow through a trapezoidal channel, which was performed in [19]. The second one is to study the unsteady behaviors of viscous fluxes around an airfoil.

4.1. Test 1 : smooth solutions

We consider the ES-BGK equations (2.1)–(3.3)

$$\begin{cases} \frac{\partial f}{\partial t} + v_x \frac{\partial f}{\partial x} = \mathcal{Q}(f), , \quad x \in (-0.5, 0.5), \ \ v \in \mathbb{R}^3, \\ f(t=0) = f_0, \end{cases}$$

with an initial datum f_0 which is a perturbation of the constant state in space and a Maxwellian distribution function in velocity, that is,

$$f_0(x, v) = \frac{\rho_0(x)}{(2\pi)} \exp\left(-\frac{|v|^2}{2}\right), \quad x \in (-0.5, 0.5), \ \ v \in \mathbb{R}^3$$

with a density $\rho_0 = 1 + 0.1\cos(2\pi x)$ and we consider pure specular reflection. Thus, the solution is expected to be smooth for large time since it does not develop any discontinuity at the boundary.

We perform several numerical simulations on a time interval $[0, t_{end}]$ with $t_{end} = 1$, a computational domain in space $I_0 = [-\pi/6, \pi/6]$ such that $(-1/2, 1/2) \subset I_0$ and a domain in velocity $\mathbf{V} = [-8, 8]^3$. Then, we choose a grid in space for I_0 constituted of $n_x = n$ points and a grid $\mathbf{V}_h$ for the velocity space with $n_v = n$ points for each direction with respectively $n = 32, 64, \ldots, n = 512$. Let us emphasize that the boundary points $x = -1/2$ and $x = 1/2$ are not exactly located on a grid

point. Since we don't know an exact solution of the problem, we compute errors with respect to a reference solution. More precisely, an estimation of the error with respect to a reference solution in L^1 norm at time T is given by

$$e_{2h} = \|f_h(T) - f_{2h}(T)\|_{L^1},$$

where f_h represents the approximation computed from a mesh of size $h = (\Delta x, \Delta v)$. The numerical scheme is said to be kth order if $e_{2h} \leqslant C\|h\|^k$, for all $0 < \|h\| \ll 1$.

In Table 1 we present the order of convergence in L^1 norm of our numerical methods at time $t = 1$, and Fig. 4 illustrates the time evolution of the e_{2h} errors with different values of h. We can clearly see the expected second order convergence. Moreover, we verify experimentally that our scheme is also second-order accurate at the boundary since with this specific boundary condition the solution is still smooth.

4.2. Test 2 : flow generated by a gradient of temperature

We consider the ES-BGK equation (2.1)–(3.3),

$$\begin{cases} \frac{\partial f}{\partial t} + v_x \frac{\partial f}{\partial x} = \frac{1}{\varepsilon}\mathcal{Q}(f), \quad x \in (-1/2, 1/2),\ v \in \mathbb{R}^3, \\ f(t=0,x,v) = \frac{1}{2\pi T_0} \exp\left(-\frac{|v|^2}{2T_0}\right), \end{cases}$$

with $T_0(x) = 1$ and we assume pure diffuse boundary conditions with $T_w(-1/2) = 1$ and $T_w(1/2) = 1.44$, which can be written as

$$f(t,x,v) = \mu(t,x) f_w(v), \text{ if } (x, v_x) \in \{-1/2\} \times \mathbb{R}^+ \text{ and } (x, v_x) \in \{1/2\} \times \mathbb{R}^-,$$

where μ is given by (2.7). This problem has already been studied in [25] using DSMC for the Boltzmann equation or using deterministic approximation using a BGK model for the Boltzmann equation in [17,6].

Here we apply our numerical scheme with the ES-BGK operator (3.3) and choose a computational domain in space $I_0 = [-0.52, 0.52]$ with only $n_x = 64$ points such that $(-1/2, 1/2) \subset I_0$ and $[-8, 8]^3$ for the velocity space with $8192 = 32 \times 16 \times 16$ grid points and the time step $\Delta t = 0.002$.

The main issue here is to capture the correct steady state for which the pressure is a perturbation of a constant state with a Knudsen layer at the boundary [17,25]. We compare our numerical solution with the one obtained with a second order classical finite volume scheme where the computational domain corresponds to the physical domain such that there is no inverse Lax–Wendroff procedure.

In Fig. 5, we represent the stationary solution (obtained approximately at time $t_{end} = 15$ for $\varepsilon = 0.3$ up to $t_{end} = 30$ for $\varepsilon = 0.1$) of the temperature and the pressure profile with both methods. The results are in a qualitative good agreement with

Table 1
Test 1 : smooth solutions. *Experimental order of convergence in L^1 norm.*

$n_x \times n_v$	L^1 error	Order	L^1 error at the boundary	Order
32^2	8.8833×10^{-4}	X	3.909×10^{-3}	X
64^2	2.5221×10^{-4}	1.94	5.832×10^{-3}	X
128^2	6.5511×10^{-5}	1.88	2.341×10^{-4}	4.1
256^2	1.7829×10^{-5}	1.91	5.811×10^{-5}	2.01
512^2	4.4571×10^{-6}	2	1.573×10^{-5}	1.89

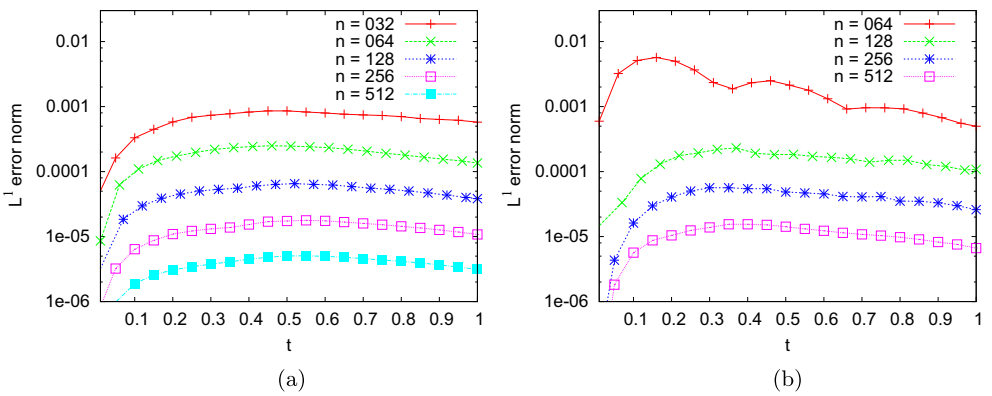

Fig. 4. Test 1 : smooth solutions. Experimental order of convergence in L^1 norm (a) in the physical domain (b) at the boundary.

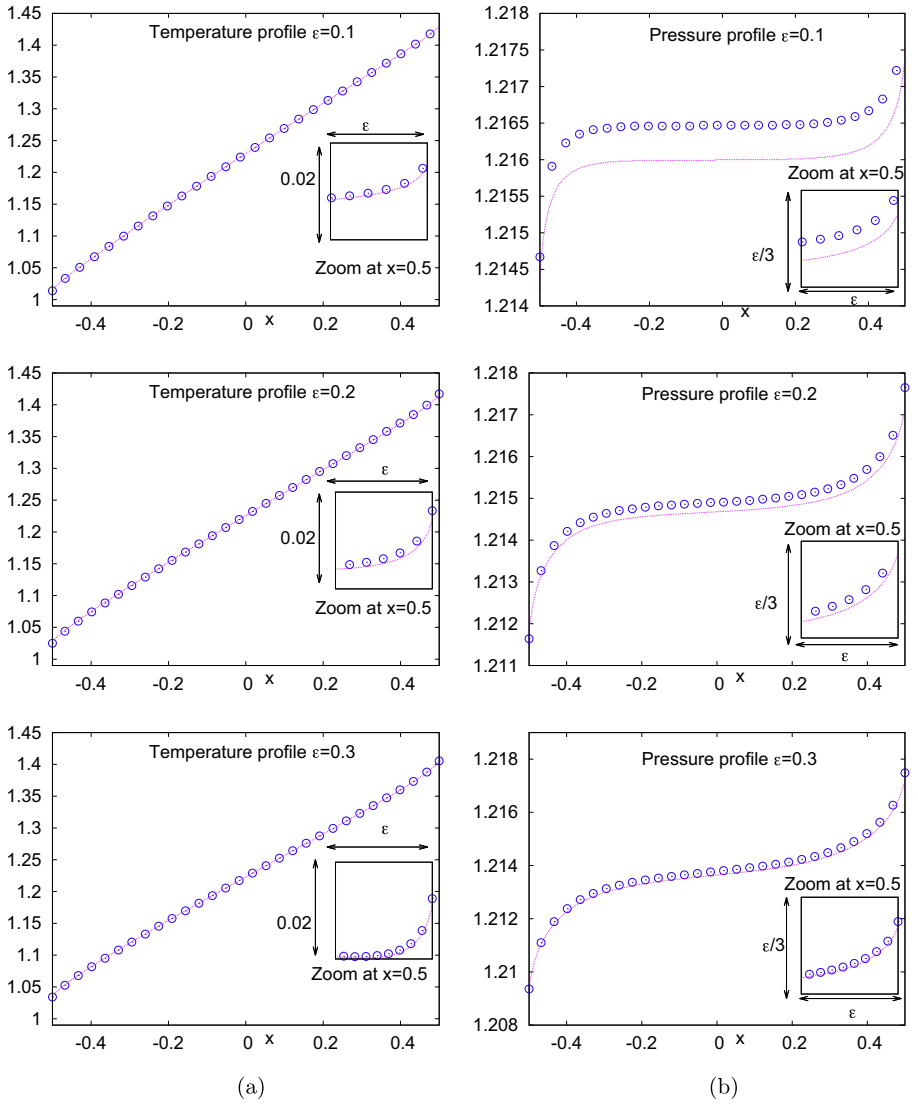

Fig. 5. Test 2 : flow generated by a gradient of temperature. comparison of steady state of (a) temperature (b) pressure for various Knudsen numbers $\varepsilon = 0.1, 0.2$ and 0.3 (– represents the numerical solution obtained with a classical second order finite volume scheme without the ILW procedure whereas ∘ represents the numerical solution obtained with the ILW procedure).

those already obtained in [25] with DSMC. More precisely, the boundary layer (Knudsen layer) appears in the density and temperature as well as the pressure, but it is small for all the quantities. The magnitude in the dimensionless density, temperature, and pressure is of order of ε and the thickness of the layer is, say $O(\varepsilon)$. In the density and temperature profiles, we cannot observe it unless we magnify the profile in the vicinity of the boundary (see the zoom in Fig. 5). Instead, since the pressure is almost constant in the bulk of the gas, we can observe perfectly the boundary layer by magnifying the entire profile. Let us emphasize that, as it is shown in Fig. 5 the Knudsen layer is a kinetic effect, which disappears in the fluid limit ($\varepsilon \to 0$).

Observe that our numerical algorithm is accurate for ε larger than 0.1, but for values below this threshold the Inverse Lax–Wendroff procedure does not give accurate results (see the steady state of the pressure) for the actual resolution. This can be easily understood since we evaluate $\mathcal{Q}(f)/\varepsilon$ at the boundary where the solution is not necessarily at equilibrium and this term does not vanish for small values ε. This can be improved by adding the limitation of the derivative (2.13) when the one given by the ILW fails (see the second item of Remark 2.1). This additional step improves the previous procedure for small values ϵ and gives better conservation (for this problem global mass is theoretically conserved, but the numerical method does not guarantee mass conservation). We present the numerical results in Fig. 6 for $\varepsilon = 0.1$ and observe the very good agreement with the reference solution.

These results provide strong evidence that the present treatment of boundary conditions using WENO extrapolation and inverse Lax–Wendroff method can be used to determine the state of a gas under highly non-equilibrium conditions. Using

deterministic methods, we can investigate the behavior of gases for situations in which molecular diffusion is important e.g., thermal diffusion.

Also let us mention that a quantitative comparison between our results ($3d_{\mathbf{v}}$ with ES-BGK operator) and [25] ($3d_{\mathbf{v}}$ Boltzmann with hard sphere potential) or [17] ($3d_{\mathbf{v}}$ BGK) gives a very good agreement on the values of the Knudsen layer and the values of the pressure inside the domain.

4.3. Test 3 : high-speed flow through a trapezoidal channel

In this section we deal with two-dimensional ES-BGK model in a trapezoidal domain. We attempt to get some steady state as

$$v_x \frac{\partial f}{\partial x} + v_y \frac{\partial f}{\partial y} = \frac{1}{\varepsilon} Q(f),$$

where $\mathbf{x} \in \Omega$ and $\mathbf{v} \in \mathbb{R}^3$. Here we will reproduce a numerical test performed in [19] but with our ILW method. The computational domain is a trapezoid

$$\Omega = \{\mathbf{x} = (x, y), \quad 0 < x < a, \ 0 < y < b + x\tan(\delta)\}$$

as shown in Fig. 7 for the parameters

$$a = 2.0, \quad b = 0.4, \quad \delta = \arctan(0.2).$$

Boundary conditions are defined separately for each of the four straight pieces

$$\partial\Omega = \Gamma_l \cup \Gamma_b \cup \Gamma_r \cup \Gamma_t$$

denoting the left, bottom, right and top parts of the boundary respectively. The bottom part represents the axis of symmetry, so we use specular reflection (2.5) there, *i.e.*

$$f(\mathbf{x}, \mathbf{v}) = (f(\mathbf{x}, \mathbf{v} - 2(\mathbf{v}\cdot\mathbf{n}(\mathbf{x}))\mathbf{n}(\mathbf{x})), \quad \mathbf{x} \in \Gamma_b, \ v_y > 0.$$

On the right part we are modeling outflow (particles are permanently absorbed), *i.e.*

$$f(\mathbf{x}, \mathbf{v}) = 0, \quad \mathbf{x} \in \Gamma_r, \ v_x < 0. \tag{3.13}$$

On the left part there is an incoming flux of particles, *i.e.*

$$f(\mathbf{x}, \mathbf{v}) = f_{\text{in}}(\mathbf{x}, \mathbf{v}) = M_{\text{in}}(\mathbf{v}), \quad \mathbf{x} \in \Gamma_l, \ v_x > 0, \tag{3.14}$$

with an inflow Maxwellian

$$M_{\text{in}}(\mathbf{v}) = \frac{\rho_{\text{in}}}{(2\pi T_{\text{in}})^{3/2}} \exp\left(-\frac{|\mathbf{v} - V_{\text{in}}|^2}{2T_{\text{in}}}\right).$$

On the top part of the boundary, we consider a diffuse reflection (2.5) of particles, with a Maxwellian distribution function

$$M_{\Gamma_t}(\mathbf{v}) = \exp\left(-\frac{|\mathbf{v}|^2}{2T_t}\right).$$

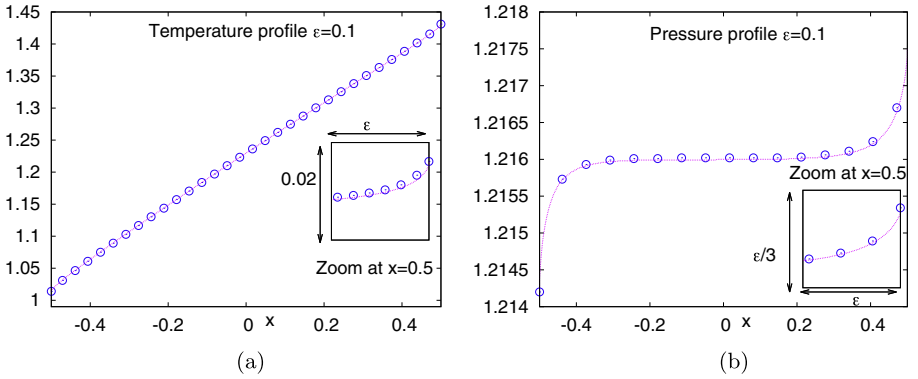

Fig. 6. Test 2 : flow generated by a gradient of temperature. comparison of steady state of (a) temperature (b) pressure for various Knudsen numbers $\varepsilon = 0.1$ represents the numerical solution obtained with a classical second order finite volume scheme without the ILW procedure whereas $\circ$ represents the numerical solution obtained with the ILW procedure and an additional limitation procedure of the derivative.

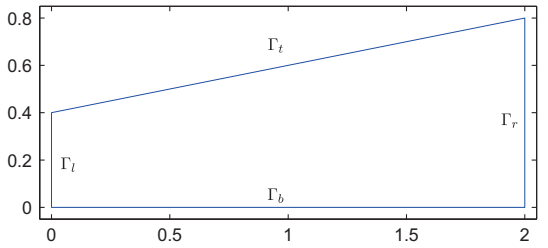

Fig. 7. Test 3 : high-speed flow through a trapezoidal channel. *Trapezoidal domain* Ω.

In the numerical experiments we assume

$$\rho_{\text{in}} = 1, \quad T_{\text{in}} = 1, \quad T_t = 1.05$$

and consider the inflow velocity in the form

$$V_{\text{in}} = \text{Mach}_{\text{in}} \sqrt{\gamma T_{\text{in}}} \begin{pmatrix} 1 \\ 0 \\ 0 \end{pmatrix},$$

where $\text{Mach}_{\text{in}} = 5$ and $\gamma = 1.4$.

To start the calculation we take an uniform initial solution equal to the values defined by the left boundary conditions:

$$f_0(\mathbf{x}, \mathbf{v}) = \frac{\rho_{\text{in}}}{(2\pi T_{\text{in}})^{3/2}} \exp\left(-\frac{|\mathbf{v} - V_{\text{in}}|^2}{2T_{\text{in}}}\right), \quad \mathbf{x} \in \Omega, \ \mathbf{v} \in \mathbb{R}^3.$$

We define the Mach number from the macroscopic quantities, computing the moments of the distribution function with respect to $\mathbf{v} \in \mathbb{R}^3$, by

$$\text{Mach} = \frac{|\mathbf{u}|}{\sqrt{\gamma T}},$$

where $c := \sqrt{\gamma T}$ is the sound speed.

We apply our inverse Lax–Wendroff method to the boundary conditions at $\partial\Omega$. More precisely, we extrapolate first the outflow at ghost points corresponding to the four straight pieces. Then we impose directly the inflow at the boundaries Γ_l and Γ_r by (3.13) and (3.14), since they are independent of outflow. While the inflow of Γ_b and Γ_t is computed by specular and diffuse reflection. Finally we use inverse Lax–Wendroff procedure to compute inflow at ghost points.

In following the sequel, numerical experiments are performed on a mesh of size 96×48 on space domain $\Omega_{\mathbf{x}}$. For velocity space we choose limit domain $[-12, 12] \times [-8, 8] \times [-8, 8]$ with the grid point number as $64 \times 48 \times 12$. Moreover for the ES-BGK operator (3.3) we choose $\nu = -0.5$. We consider the weak collision case, *i.e.* $\text{Kn} = 5$. In Figs. 8–10, we show on the left hand side, the contour plots of the density, the temperature and the Mach number while the right hand side plots show the absolute values of these quantities plotted along the axis of symmetry $y = 0$. We observe that the Mach number reaches its maximum at Γ_r. We can observe also that there is a clear maximum of the density near $x = 0.75$. In the same region the temperature reaches its maximum. All these results coincide with that in [19] implemented by DSMC method.

4.4. Test 4 : high-speed flow around an object

In this section, we desire to simulate viscous fluxes around an airfoil (see Fig. 11). In literature [16], the unsteady behaviors of viscous fluxes were studied using unsteady compressible Navier-Stokes equations. No slip boundary condition were used on the airfoil surface, *i.e.* $\mathbf{u} = 0$. In fact, there are instances wherein under certain angles of attack the flow becomes

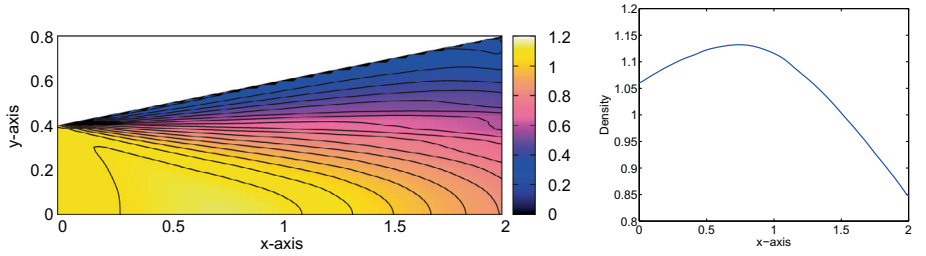

Fig. 8. Test 3 : high-speed flow through a trapezoidal channel. *Stationary state of the density with* $\varepsilon = 5$.

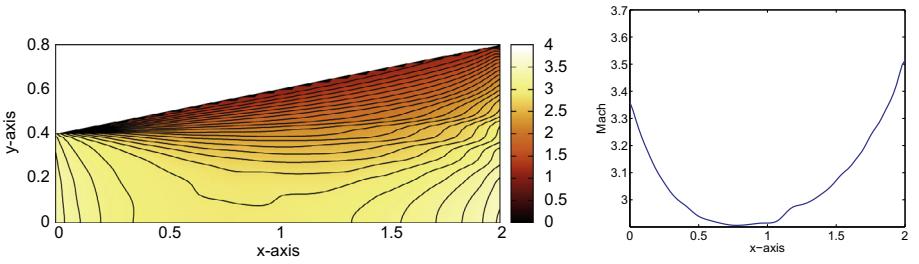

Fig. 9. Test 3 : high-speed flow through a trapezoidal channel. *Stationary state of the Mach number with* $\varepsilon = 5$.

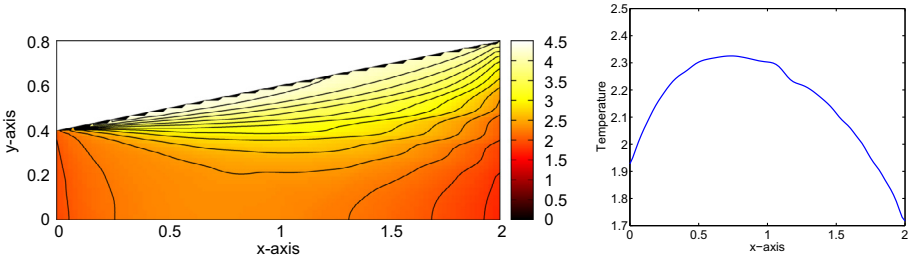

Fig. 10. Test 3 : high-speed flow through a trapezoidal channel. *Stationary state of the temperature with* $\varepsilon = 5$.

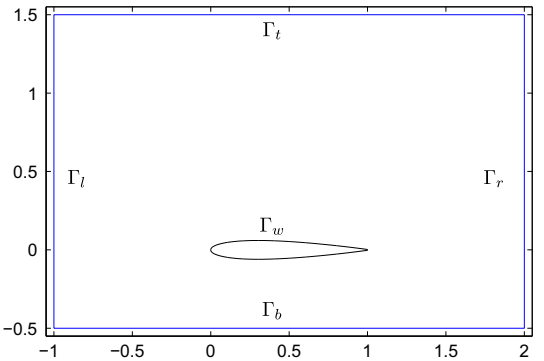

Fig. 11. Test 4 : high-speed flow around an object. *Domain including an airfoil.*

unsteady and the compressible Navier-Stokes equations do not lead to any convergent steady-state solution. Here we use ES-BGK model to reproduce this unsteady behaviors.

In [16], the computations were performed with Mach number Ma $= 0.3$ and Reynolds number Re $= 3000$. The Mach, Reynolds and Knudsen numbers relation is given by:

$$\mathrm{Kn} = \frac{\mathrm{Ma}}{\mathrm{Re}}\sqrt{\frac{\gamma\pi}{2}},$$

where $\gamma = 1.4$ is the ratio of specific heats. Therefore we have a very small Knudsen number approximately equal to Kn $= 0.0001$. As we mentioned in Remark 2.2, the inverse Lax–Wendroff procedure alone is not appropriate in this case. We thus supplement it with use the WENO type extrapolation (2.13) to stabilize the inverse Lax–Wendroff procedure.

The boundary is divided in two parts: the rectangle $\Gamma_{\mathrm{ext}} = \Gamma_l \cup \Gamma_b \cup \Gamma_r \cup \Gamma_t$ and the airfoil profile Γ_w. We impose inflow on Γ_{ext} as follows

$$f(\mathbf{x},\mathbf{v}) = \frac{\rho_{\mathrm{in}}}{2\pi T_{\mathrm{in}}}\exp\left(-\frac{|\mathbf{v}-V_{\mathrm{in}}|^2}{2T_{\mathrm{in}}}\right), \quad \mathbf{n}(\mathbf{x})\cdot\mathbf{v} \geqslant 0,\ \mathbf{x}\in\Gamma_{\mathrm{ext}},$$

where the parameters $\rho_{\mathrm{in}},\ T_{\mathrm{in}},\ v$ have the same values as in the previous test, and we and consider the inflow velocity in the form

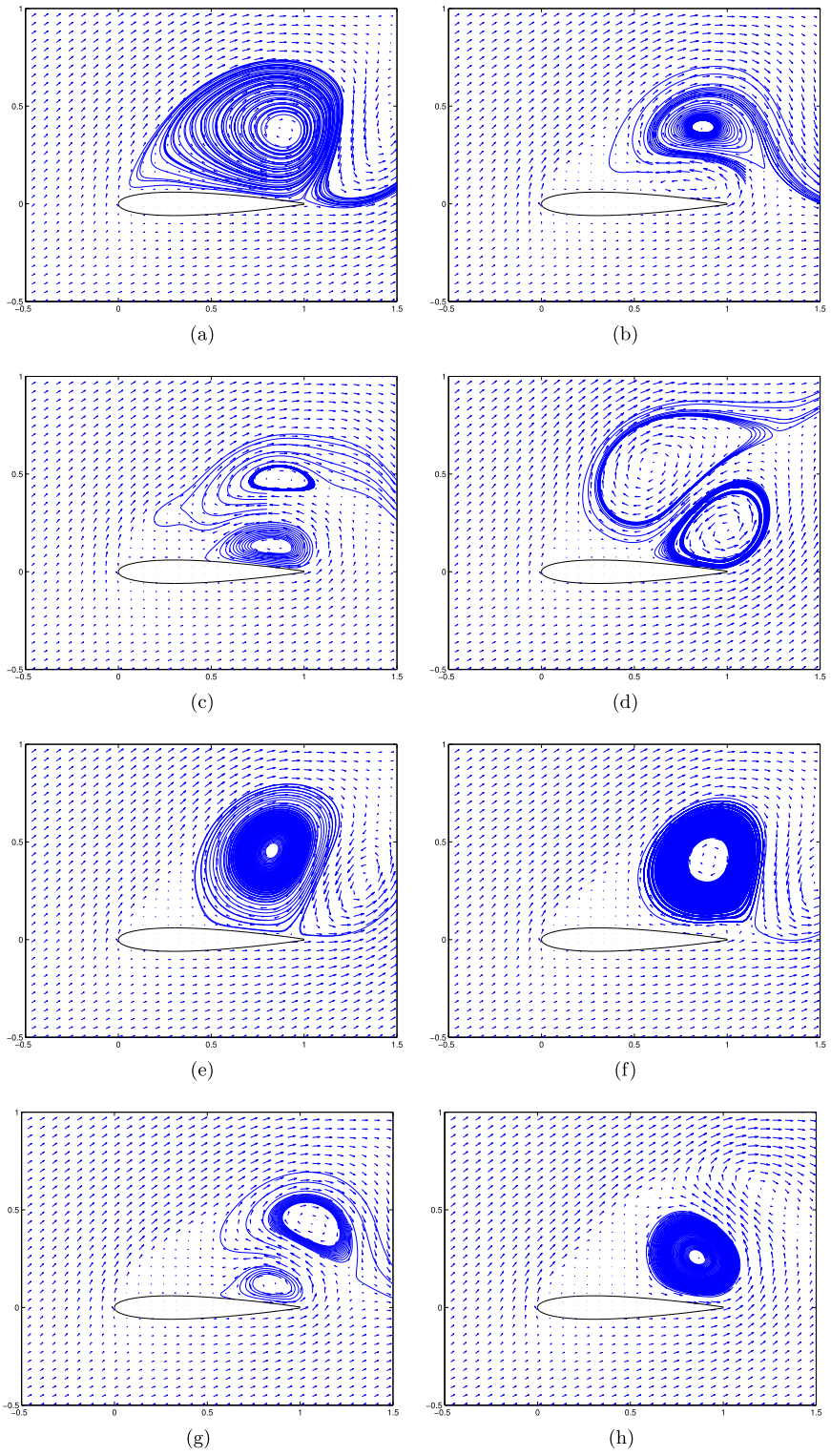

Fig. 12. Velocity vector and streamline plot around an airfoil.

$$V_{\text{in}} = \text{Ma}\sqrt{\gamma T_{\text{in}}}\begin{pmatrix}\cos(\lambda)\\ \sin(\lambda)\\ 0\end{pmatrix},$$

with the angle $\lambda = 30^\circ$. Finally on Γ_w, we use the pure specular reflection boundary conditions.

To perform this simulation, we consider an uniform mesh of size 180×180 in domain Ω. We use a limited velocity domain $[-8,8]^2$ with mesh size 40×40. We compare evolution of vortex in a periodic unsteady cycle with the one performed with unsteady Navier–Stokes equation [16]. We present a unsteady cycle in Fig. 12. In Fig. 12(a), there is a long bubble covering the entire upper surface. In Fig. 12(b) and (c), a small vortex is induced at the trailing edge and it grows in size and strength. In Fig. 12(d), two counter rotating vortices form with one of them at the trailing edge and other near the middle region. In Fig. 12(e), the right vortex is lifted and is collapsed since the left one is increasing in size and strength. In Fig. 12(f), the vortex lift increases due to formation of new bubble with single clockwise vortex trapped inside and anti-clockwise vortex shed from the trailing edge. In Fig. 12(g), two vortices form on clockwise and there is a dead air region above the upper surface. In Fig. 12(h), at trailing edge the vortex grows in strength and the dead air region is lifted by a new vortex near the trailing edge, which will finally become a long bubble covering again the entire upper surface. It is interesting to note that although the Boltzmann type model is used here, we are able to observe a similar behavior as in [16].

5. Conclusion

In this paper we present an accurate method to deal with kinetic models set in an arbitrary geometry using a Cartesian grid. We reconstruct the distribution function f on ghost points to discretize the transport operator. For this we proceed in three steps: first extrapolate the distribution function f on ghost points for outflow and then apply boundary conditions to compute the inflow at the boundary. Finally we implement an inverse Lax–Wendroff procedure to give an accurate approximation of f for inflow on the ghost points. One-dimensional examples are given to show that this method has second order accuracy in L^1 norm. Moreover several numerical simulations in $1D \times 3D$ and $2D \times 3D$ illustrate that our method can reproduce similar results as the ones in literature. An extension of the inverse Lax–Wendroff method to moving boundary is in progress.

Acknowledgments

The authors want to thank the anonymous referees for their suggestions of the application of the WENO extrapolation together with the inverse Lax–Wendroff procedure in Test 2 for small values of ε.

References

[1] P. Andries, P.Le. Tallec, J. Perlat, B. Perthame, The Gaussian-BGK model of Boltzmann equation with small Prandtl numbers, European Journal of Mechanics B/Fluids 63 (1991) 323–344.
[2] P.A. Berthelsen, O.M. Faltinsen, A local directional ghost cell approach for incompressible viscous flow problems with irregular boundaries, Journal of Computational Physics 227 (9) (2008) 4354–4397.
[3] P.L. Bhatnagar, E.P. Gross, M. Krook, A model for collision processes in gases. Small amplitude processes in charged and neutral one-component systems, Physical Reviews 94 (1954) 511–525.
[4] C. Cercignani, The Boltzmann Equation and Its Applications, Springer-Verlag, Berlin, 1988.
[5] F. Filbet, E. Sonnendrücker, Comparison of Eulerian Vlasov solvers, Computer Physics Communications 150 (2003) 247–266.
[6] F. Filbet, On deterministic approximation of the Boltzmann equation in a boundary domain, Multiscale Modeling and Simulation 10 (2012) 792–817.
[7] F. Filbet, S. Jin, A class of asymptotic preserving schemes for kinetic equations and related problems with stiff sources, Journal of Computational Physics 229 (20) (2010).
[8] F. Filbet, S. Jin, An asymptotic preserving scheme for the ES-BGK model of the Boltzmann equation, Journal of Scientific Computing 46 (2) (2011) 204–224.
[9] F. Filbet, T. Rey, A rescaling velocity method for dissipative kinetic equations applications to granular media, submitted for publication.
[10] L.H. Holway, Kinetic theory of shock structure using an ellipsoidal distribution function, Proceedings of the Fourth International Symposium on Rarefied Gas Dynamics, University of Toronto, 1964, vol. I, Academic Press, New York, 1966, pp. 193–215.
[11] L. Huang, C.-W. Shu, M. Zhang, Numerical boundary conditions for the fast sweeping high order WENO methods for solving the Eikonal equation, Journal of Computational Mathematics 26 (2008) 336–346.
[12] D.M. Ingram, D.M. Causon, C.G. Mingham, Developments in Cartesian cut cell methods, Mathematics and Computers in Simulation 61 (2003) 561–572.
[13] G.-S. Jiang, C.-W. Shu, Efficient implementation of weighted ENO schemes, Journal of Computational Physics 126 (1996) 202–228.
[14] Lai Ming-Chih, Charles S. Peskin, An immersed boundary method with formal second-order accuracy and reduced numerical viscosity, Journal of Computational Physics 160 (2) (2000) 705–719.
[15] J.C. Maxwell, Philosophical Transactions of the Royal Society of London 70 (1867) 231.
[16] P.S. Murthy, V.S. Holla, H. Kamath, Unsteady Navier–Stokes solutions for a NACA 0012 airfoil, Computer Methods in Applied Mechanics and Engineering 186 (2000) 85–99.
[17] T. Ohwada, Investigation of heat transfer problem of a rarefied gas between parallel plates with different temperatures, in: C. Shen (Ed.), Rarefied Gas Dynamics, Peking University, 1996, pp. 217–234.
[18] C.S. Peskin, Flow patterns around heart valves. A numerical method, Journal of Computational Physics 10 (1972) 252–271.
[19] Sergej Rjasanow, Wolfgang Wagner, Stochastic Numerics for the Boltzmann Equation, Springer, 2005.
[20] G. Russo, F. Filbet, Semi-Lagrangian schemes applied to moving boundary problems for the BGK model of rarefied gas dynamics, Kinetics and Related Models 2 (1) (2009) 231–250.
[21] S. Tan, C.-W. Shu, Inverse Lax–Wendroff procedure for numerical boundary conditions of conservation laws, Journal of Computational Physics 229 (2010) 8144–8166.

[22] S. Tan, C. Wang, C.-W. Shu, J. Ning, Efficient implementation of high order inverse Lax–Wendroff boundary treatment for conservation laws, Journal of Computational Physics (2012) 2510–2527.
[23] B. van Leer, Towards the ultimate conservative difference scheme. II. Monotonicity and conservation combined in a second order scheme, Journal of Computational Physics 14 (1974) 361–370.
[24] T. Xiong, M. Zhang, Y.-T. Zhang, C.-W. Shu, Fifth order fast sweeping WENO scheme for static Hamilton–Jacobi equations with accurate boundary treatment, Journal of Scientific Computing 45 (1–3) (2010).
[25] D.J. Rader, M.A. Gallis, J.R. Torczynski, W. Wagner, Direct simulation Monte Carlo convergence behavior of the hard-sphere-gas thermal conductivity for Fourier heat flow, Physics Fluids 18 (2006) 077102.